

# The Weizmann Supercooled Droplets Observation on a Microarray (WISDOM) and application for ambient dust

Naama Reicher, Lior Segev, Yinon Rudich

Department of Earth and Planetary Sciences, The Weizmann Institute of Science, Rehovot, Israel

*Correspondence:* Naama Reicher ([naama.reicher@weizmann.ac.il](mailto:naama.reicher@weizmann.ac.il)), Yinon Rudich ([yinon.rudich@weizmann.ac.il](mailto:yinon.rudich@weizmann.ac.il))

**Abstract.** The Weizmann Supercooled Droplets Observation on Microarray (WISDOM) is a new setup for studying ice nucleation in an array of monodisperse droplets for atmospheric implications. WISDOM combines microfluidics techniques for droplets production and a cryo-optic stage for observation and characterization of freezing events of individual droplets. This setup is designed to explore heterogeneous ice nucleation in the immersion freezing mode, down to the homogeneous freezing of water (235 K) in various cooling rates (typically  $0.1\text{-}10\text{ K min}^{-1}$ ). It can also be used for studying homogeneous freezing of aqueous solutions in colder temperatures. Frozen fraction, ice nucleation active surface site (INAS) densities and freezing kinetics can be obtained from WISDOM measurements for hundreds of individual droplets in a single freezing experiment. Calibration experiments using eutectic solutions and previously studied materials are described. WISDOM also allows repeatable cycles of cooling and heating for the same array of droplets. This paper describes the WISDOM setup, its temperature calibration, validation experiments and measurement uncertainties. Finally, application of WISDOM to study the INP properties of size-selected ambient Saharan dust particles is presented.

## 1 Introduction

In mixed phase clouds, water droplets remain stable in a supercooled state below 273 K and ice nucleates spontaneously as droplets reach the homogeneous freezing temperature, below 236 K (Pruppacher et al., 1998). At warmer temperatures, ice particles may coexist with supercooled droplets, due to heterogeneous nucleation facilitated by the presence of ice nuclei particles (INPs)(Cantrell and Heymsfield, 2005). In cases where INPs are immersed in the droplet before supercooling, referred to as immersion freezing mechanism, the droplets first grow to supercritical size before freezing occurs (de Boer et al., 2011). Observations and modeling studies suggest that immersion freezing is the prominent mechanism for heterogeneous ice formation in mixed phase clouds (Ansmann et al., 2008; Field et al., 2012; Nagare et al., 2016; Possner et al., 2017; Rosenfeld and Woodley, 2000).

Ice particles affect the radiative and microphysical properties of mixed phase clouds and Earth's hydrological cycle. Therefore, they can influence present and possibly future climate (Hoose and Möhler, 2012; IPCC, 2013). Studying ice formation in clouds is hence important, and yet, due to its complexity, this process is still not fully understood and presents a

30 great challenge to laboratory and field researchers as well as for clouds and climate modelers (DeMott et al., 2010; Schnaiter  
31 et al., 2016; Ullrich et al., 2017).

32 Offline studies of immersion freezing often use cold stage techniques (Budke and Koop, 2015). The basic idea is to place an  
33 array of droplets over a cold stage and cool continuously until all are frozen, to obtain a quantitative measurement of their  
34 corresponding freezing temperatures (Vali, 1971). The droplets may be microliter-sized and observed with a simple camera.  
35 Smaller droplets, down to the pico-liter range, are usually observed under a microscope. In both cases, freezing events are  
36 identified by optical changes in the droplets when they crystalize (Atkinson et al., 2013; Hiranuma et al., 2015; Knopf and  
37 Lopez, 2009; Murray et al., 2011).

38 Cold stage techniques may suffer from technical issues such as droplets evaporation and vapor transfer due to the Wegener–  
39 Bergeron–Findeisen process, where ice grows on the expense of supercooled droplets or from seeding of neighboring  
40 droplets by formation and surface growth of frost halos (Budke and Koop, 2015). Some cold stages instruments place oil  
41 over the droplets or use droplet in oil emulsions to prevent these effects (Murray et al., 2012). Still, results from cold stage  
42 experiments may be biased by effects of inhomogeneous temperature of the substrate and the surroundings or by various  
43 contaminations caused during droplets’ preparation and measurement (Hiranuma et al., 2015). Furthermore, supercooling is  
44 limited due to the presence of impurities, which increases with the volume of the droplet. Hence, to allow comprehensive  
45 studies down to the homogeneous region, low volumes ( $<1 \mu\text{L}$ ) are used and generation of these volumes is not trivial and  
46 may cause further complications.

47 Microfluidics is a technology of fluids manipulation in micro-channels array on a small device. Microfluidics is widely used  
48 in a range of fields, such as physics, chemistry, biology, life sciences and the food industry (Neethirajan et al., 2011;  
49 Sackmann et al., 2014; Whitesides, 2006). Recent studies used microfluidic apparatus to study ice nucleation processes.  
50 Riechers et al. (2013) used a microfluidics device to produce and collect monodisperse droplets of water in various sizes,  
51 which were subsequently observed under a microscope to study their homogeneous freezing. Stan et al. (2009) recorded  
52 nucleation in water droplets and silver iodide seeded droplets, while droplets were flowing during cooling. Schmitz et al.  
53 (2009) established ‘Dropspots’, a static microfluidic array of droplets, later used by Edd et al. (2009) to measure nucleation  
54 kinetics. However, in the atmospheric heterogeneous ice nucleation field, microfluidics techniques are not widely adopted,  
55 despite many potential advantages.

56 The WeIzmann Supercooled Droplets Observation on Microarray (WISDOM) is a new instrument combining the cold stage  
57 technique with microfluidics technology, and is designed to study immersion freezing of micrometer-sized droplets, while  
58 addressing most of the technical issues listed above. The WISDOM setup introduces several advantages of microfluidics to  
59 the atmospheric ice nucleation field. WISDOM is based on the ‘Dropspots’ static array (Schmitz et al., 2009), which enables  
60 the separation and the fixation of the droplets, so that each individual droplet is recorded and studied, and also can be used  
61 for repetition of freezing cycles and further exploration of the nucleation process of a specific sample.

62 In this paper, we present the WISDOM setup, its calibration and validation procedures. For validation experiments,  
63 homogeneous and heterogeneous freezing were examined by following homogeneous freezing rates of pure aqueous or

64 solutions or deriving the efficiencies of three types of mineral dust surrogates and collected ambient Saharan dust to validate  
65 heterogeneous freezing experiments.

66 Homogeneous nucleation rates are described stochastically using the volume-dependent ice nucleation rate ( $J_v(T)$ ) in  
67 supercooled droplets, given by the frozen fraction ( $f_{ice}$ ) of droplets with volume  $V$  at a certain temperature ( $T$ ) and time  
68 intervals ( $\Delta t$ ) (Alpert et al., 2011; Murray et al., 2010; Riechers et al., 2013),

$$69 \quad J_v(T) = \frac{-\ln(1-f_{ice}(T))}{V\Delta t}, \quad (1)$$

70 Heterogeneous freezing is described by a singular approach that assumes that nucleation occurs at a certain temperature due  
71 to special nucleation site. Hence, a cumulative number of nucleation sites per unit surface area,  $n_s$ , is used to describe the  
72 heterogeneous nucleation efficiency at a certain temperature,

$$73 \quad n_s(T) = \frac{-\ln(1-f_{ice}(T))}{A}, \quad (2)$$

74 Where  $f_{ice}$  is the fraction of frozen droplets at temperature  $T$ , and  $A$  is the specific surface area of the immersed particles in  
75 each droplet (Vali, 1971; Vali et al., 2015; Whale et al., 2015).

76 Validation of WISDOM was further extended below the homogeneous nucleation temperature of pure water, using aqueous  
77 solutions as the freezing temperatures of solutions decrease as a function of the solution water activity.

## 78 **2 Experimental setup**

### 79 **2.1 Droplets production and trapping**

80 The WISDOM setup, shown in Figure 1, is made of a microfluidic setup which include a pressure controlled pump with 4  
81 independent flow channels (OB1 MK3 by Elveflow), a stereoscope (SMZ-171 by Motic) that permits a full view of all  
82 channels and inlets, and a CCD camera (GS3 by Point Grey) that enable real time monitoring of the droplets production. The  
83 flows in the channels are continuous and controlled by the pressure pump. One channel is connected to the continuous (oil)  
84 phase, and a second channel contains the sample (aqueous solution that can contain INPs). The two phases meet in a narrow  
85 junction where monodisperse droplets are generated due to the pressure exerted by one phase over the other. The ratio  
86 between the flows determines the size of the emerging droplets; the volume increases with increasing flow rate of the  
87 sample. In this setup, droplets are suspended in an oil mixture, consisting of mineral oil (Sigma Aldrich) and a 2 weight  
88 percent (wt%) nonionic surfactant (span80®, Sigma Aldrich), added for droplets stabilization (Riechers et al., 2013). Hence,  
89 an array of picoliter (micrometer-size) droplets is generated directly on a device.

90 The principle of the Schmitz et al. (2009) design is that the droplets flow into round chambers that are connected by  
91 constriction channel. At a certain flow, the droplets are squeezed through the constriction channel and the array fills up with  
92 droplets. When the flow is too weak or stopped, the constriction channel stops the droplets' movement and they are trapped  
93 in the chambers. The droplets are isolated and stable in the chambers and it is safe to move the device from the generation  
94 stage to the cold stage for the freezing experiments.

95 Devices are fabricated following the Schmitz et al. (2009) protocol. Briefly, the device pattern is imprinted on a  
96 polydimethylsiloxane (PDMS) polymer, later glued to a 1mm thick microscope glass slide using air plasma treatment. After  
97 the plasma treatment the PDMS surfaces are hydrophilic (Eddings, 2008). Therefore, the devices were used only in the  
98 following day, after their surfaces became hydrophobic, following their exposure to the atmosphere, or after their annealing  
99 at 60°C for half an hour.

## 00 **2.2 Freezing experiments and detection**

01 The droplets array is placed in a commercial cryostage (Linkam, THMS600) coupled to an optical microscope (Olympus,  
02 BX-51 with 10X magnification, transmission mode). Experiments are monitored by a microscope mounted CCD camera  
03 (Allied Vision Technologies, Oscar F-510C) for automatic identification of droplets and their freezing events. Both the  
04 device and the cooling stage are cleaned with 2-propanol. Then the device is placed over the stage together with a thin layer  
05 of oil on its bottom to provide good thermal conductivity. Each freezing experiment starts with dry N<sub>2</sub> purging to replace the  
06 moist atmosphere inside the cryostage to prevent condensation. During the experiment, N<sub>2</sub> flow prevents water condensation  
07 on the cryostage window. Freezing experiments are conducted with a cooling rate of 1 K min<sup>-1</sup> which is relevant for  
08 atmospheric conditions and also allows good thermalization of the droplets, as will be shown in the calibration section  
09 (section 3.1). Each cooling cycle is followed by a heating cycle, where melting is observed. Analysis of the melting onset is  
10 then used to verify that the thermal conductivity is good and thus validate the measurement.

11 In-house LabVIEW software is used to record a freezing experiment movie file and analyze it offline. The temperature  
12 readings by the Linkam cryostage temperature sensor ( $\leq \pm 0.25$  K for the operated temperature range) and the movie frames  
13 are synchronized and integrated. In most cases, 1 second (or 0.017 K at 1 K min<sup>-1</sup>) per frame is used. Currently, the  
14 WISDOM setup operates with two types of devices that differ in their droplets' trap diameter: 40  $\mu\text{m}$  and 100  $\mu\text{m}$ .  
15 Approximately 550 and 120 droplets can be monitored per experiment in the smaller and larger diameter devices,  
16 respectively. Statistically, for the same sample, larger droplets encompass more INP surface area within each droplet, which  
17 can be more sensitive for detecting rare active sites. The device can be reused for the same sample, if it is not clogged or  
18 destroyed during the experiment. However, because the channels of the 40  $\mu\text{m}$  device are smaller they tend to clog faster (for  
19 instance by large particles).

## 20 **2.3 Automatic detection of phase transitions**

21 The optical brightness of a droplet changes during a phase transition (freezing or melting) due to the different interaction of  
22 light with the liquid and the solids. For phase transition detection, an in-house image processing LabVIEW program  
23 monitors automatically the optical brightness change. The program detects the droplets using a spherical shape criterion and  
24 sets a square surrounding the droplet that defines an array of pixels that are attributed to that specific droplet. A change in the  
25 optical brightness is represented by the gray level value of the image's pixels, ranging from 0 to 255. Freezing is calculated  
26 per movie frame and is defined as the subtraction of the brightness mean value for each droplet in two consecutive frames

27 ( $\Delta GL$ ), thus allowing derivation of freezing rates. At the beginning of the analysis, the first 15 frames are used to identify the  
28 noise level of the signal by calculating its standard deviation  $\text{std}(\Delta GL)$ . The program then searches for the maximal freezing  
29 signal that is also greater than 5 times the noise level. The temperature associated with this freezing signal is assigned as the  
30 freezing temperature for that droplet.

31 In this algorithm, the program can distinguish successfully between a phase transition event and noise that arises from the  
32 camera signal, droplet movement or any other interruption. Figure 2 presents a spectral analysis for different types of phase  
33 transitions observed in WISDOM. Since WISDOM operates in transmission microscopy mode, the light is scattered more  
34 efficiently by ice crystals in comparison with a liquid droplet and a freezing event involves droplet darkening and a negative  
35 signal. The negative signal of a freezing event of a single droplet is shown in Figure 2a. In comparison, during melting, the  
36 droplet becomes brighter until all the crystals melt, and the signal is positive. In Figure 2b+c the analysis of a melting signal  
37 and a eutectic melting signal are presented for the entire frame.

### 38 **3 Results and WISDOM validation**

#### 39 **3.1 Temperature calibration**

40 Temperature accuracy is a most important parameter in ice nucleation experiments. An error propagation analysis by  
41 Riechers et al. (2013) demonstrated how the temperature uncertainty may lead to a distribution of temperatures between  
42 different instruments. Therefore, we performed a thorough temperature calibration using the known eutectic melting points  
43 and the melting points of several aqueous solutions as calibration reference points. Although ice nucleation experiments are  
44 performed while cooling, the calibration experiments were done while heating to improve the calibration precision and to  
45 avoid biases associated with supercooling of the liquids (Budke and Koop, 2015).

##### 46 **3.1.1 Droplets thermalization**

47 The temperature of the Linkam stage was measured at the upper center part of the cooling stage and hence may differ from  
48 the actual temperature of the droplets in the device due to thermal effects such as temperature gradients and temperature lag.  
49 During cooling or heating, a vertical temperature gradient may develop between the top of the device, in contact with the  
50 inner ambient of the cryostage, and the bottom of the device, which is in contact with the cooling silver block. This gradient  
51 is expected to increase in magnitude, as the temperature of the stage decreases or increases below or above ambient  
52 temperature. Edd et al. (2009) used a similar setup and found a difference between the top temperature and the bottom  
53 temperature of about 2 K around 237 K and 3 K around 227 K. Stan et al. (2009) also reported a vertical gradient of 1-2 K,  
54 that was reduced to 0.5 K with a flow of cooled  $N_2$  over their device. In addition, a thermal lag may arise during cooling or  
55 heating as the rate of temperature change is high and precludes proper temperature equilibration. Hence, a more accurate  
56 measurement of the droplet temperature is taken as a sum of the stage temperature with the contributions of both thermal  
57 gradient and lag.

58 Figure 3 demonstrates the combined effects of temperature change rate and device properties on the thermalization of pure  
59 water droplets (double distilled, 18.2 M $\Omega$  cm). Specifically, freezing and melting experiments at different rates were  
60 performed. The temperature difference ( $\Delta T$ ) is the difference between the measured values and the extrapolated temperature  
61 at equilibrium conditions (0 K min<sup>-1</sup>). As expected, at slower temperature cooling (heating) rates, the droplets are more  
62 equilibrated with the stage temperature and  $\Delta T$  is negligible. However,  $\Delta T$  increases at higher temperature cooling (heating)  
63 rates (e.g.; 10 K min<sup>-1</sup>). We observed that during cooling (heating) the droplet is warmer (colder) than the stage and will  
64 freeze (melt) at colder (warmer) temperature at higher cooling (heating) rates. We also found that because  $\Delta T$  is higher, in  
65 absolute value, for devices of thicker PDMS and/or in devices which hold larger droplets, it should be considered in the final  
66 temperature calibration for these scenarios. Furthermore,  $\Delta T$  was found to be almost symmetric for higher temperature  
67 cooling (heating) rates. However, for 1 K min<sup>-1</sup>,  $\Delta T$  during cooling is higher than that for heating. Our conjecture is that this  
68 can be an effect of the higher thermal gradient that develops as the temperature decreases well below ambient (236 K).

### 69 **3.1.2 Melting of aqueous solutions**

70 Figure 4 presents the measured melting points of NaCl solutions with different water activities. Reported melting points  
71 represent the temperature in which all ice crystals in the droplets completely melted, in contrast with melting temperatures  
72 reported for pure liquids such as water, where the onset of melting is defined as the melting point. Melting temperature  
73 results were consistent with theoretical melting temperatures reported in Koop and Zobrist (2009). This provides support to  
74 our conclusion that droplets thermalize with the cooling stage when using a heating rate of 0.1-1 K min<sup>-1</sup>. For faster heating  
75 rates (i.e. 10 K min<sup>-1</sup>), the thermal lag was more pronounced, leading to a melting point shift of about 2-3 K. For more  
76 concentrated solutions, faster heating rates shifted the melting points more.

### 77 **3.1.3 Melting of eutectic solutions**

78 Some aqueous solutions, such as NaCl and MgCl<sub>2</sub>, arrange in a super-lattice at a certain wt% to form a solid with a well-  
79 defined melting point (eutectic) (252.05 K for NaCl and at 239.95 K for MgCl<sub>2</sub>) (Borgognoni et al., 2009; Farnam et al.,  
80 2016). Interestingly, this type of melting has a smaller optical signature compared to that of melting points of pure  
81 substances, as can be seen in Figure 2b. We have set a specific water activity for a solution by determining its quantitative  
82 composition using the extended aerosol inorganic model (E-AIM) (Clegg et al., 1998) at room temperature (298 K). For  
83 calibration purposes, because eutectic melting had a negligible variation for different water activities used in the range of  
84 0.99 to 0.95, we decided to take their average to achieve a single melting value. These eutectic melting temperatures are  
85 colder than the melting point of pure water and, therefore, are used for expanding WISDOM calibration range.

86 The final calibration is obtained for a device with a specific PDMS thickness and at a specific cooling (heating) rate. For  
87 example, devices with 100  $\mu$ m diameter sized droplet and of 4mm PDMS thickness have a linear calibration curve of  
88  $T_{\text{drop}}=0.97\times T_{\text{stage}}-0.46$  at 0.1 K min<sup>-1</sup>.

### 89 3.2 Measurement reproducibility and device variability

90 Device's inter-variability was determined from 20 devices by comparing their corresponding homogeneous freezing  
91 temperatures of pure water. Specifically, each device was recycled three times with freshly prepared droplets. Our results  
92 showed high reproducibility in the median freezing temperature, where 50% of the probed droplets froze ( $T_{50}$ ), and high  
93 reproducibility in the melting point temperature. Variation within devices was always smaller than  $\pm 0.2$  K at  $1$  K  $\text{min}^{-1}$  and  
94  $0.1$  K  $\text{min}^{-1}$  (variation within the devices over the whole freezing range is presented in Appendix A).

### 95 3.3 Homogeneous freezing rates of pure water

96 Homogeneous nucleation in supercooled water occurs in WISDOM between 238 and 237 K for a cooling rate of  $1$  K  $\text{min}^{-1}$   
97 and droplets diameter of  $100$   $\mu\text{m}$ . Figure 5 shows WISDOM nucleation rates in comparison with other similar instruments. It  
98 is seen that the slope of the rate and temperatures are similar to the slopes reported for other instruments. The temperature  
99 where 50% of droplets froze ( $T_{50}$ ) is also in the expected range according to model results of Hoffer (1961). WISDOM rates  
00 are slightly slower, but within the uncertainty of the instruments used by Riechers et al. (2013) and Stan et al. (2009).  
01 Stöckel et al. (2005) show a higher nucleation rate. This discrepancy can be explained by a decrease in the number of surface  
02 nucleation events due to the oil phase surrounding our droplets, whereas in Stöckel et al. (2005), droplets are suspended in  
03 air which allows surface nucleation may occur.

### 04 3.4 Homogeneous and heterogeneous freezing of aqueous solutions

05 The water-activity-based ice nucleation theory by Koop et al. (2000) describes the dependence of the freezing temperature  
06 depression on the water activity ( $a_w$ ) of the solution, regardless of the solute nature. Figure 6 presents the theoretical freezing  
07 and melting temperature curves from Koop et al. (2000) with homogeneous ice nucleation results measured in WISDOM, for  
08 four solutions with atmospheric relevance. Water activities for NaCl, ammonium sulfate (AS), glucose and levoglucosan  
09 mixtures were derived from the AIM model and were corrected for glucose and levoglucosan, for which water activity is  
10 temperature dependent (Knopf and Lopez, 2009; Zobrist et al., 2008). The experiments were conducted at  $1$  K  $\text{min}^{-1}$  for  $40$   
11 and  $100$   $\mu\text{m}$  droplet diameters. The results follow the theoretical curves of the water-activity-based ice nucleation, and the  
12 dependence of the homogeneous freezing on the droplet volume is as expected (Hoffer, 1961; Kuan-Ting and Wood, 2016)  
13 as the curve of the smaller diameter droplets (green curve) is slightly colder compared with the larger volume droplets (dark  
14 green curve).

15 Similar experiments were conducted for  $0.1$  wt% of Arizona Test Dust particles (ATD, Powder Technology Inc.) immersed  
16 in glucose solution droplets. The ATD particles facilitate the ice nucleation at warmer temperatures, in agreement with  
17 similar studies (Hartmann et al., 2011; Niedermeier et al., 2010), and the freezing depression follow the water-activity-based  
18 ice nucleation curves. Here, the dependence of the freezing point on the droplet volume is more pronounced, as the surface

19 area of the immersed particles is higher, hence they contain higher number of nucleation sites (Marcolli et al., 2007) as will  
20 be shown in the next section for two more types of dust.

21 Below 223 K, ice nucleation occurs at slightly lower temperatures than expected by the theoretical freezing curve. As the  
22 WISDOM temperature calibration is not valid in this temperature range, we cannot conclude if this is due to a change of the  
23 thermal conductivity of the device or an effect of the high concentration of the solute in the water.

24

### 25 **3.5 Heterogeneous nucleation and $n_s$ spectra of INP in pure water**

#### 26 **3.5.1 Standard dust powder**

27 Heterogeneous freezing efficiencies of suspended mineral dusts K-Feldspar and Illite-NX in supercooled water droplets are  
28 presented in Figure 7 and summarized in Table 1, and are compared to recent published data. The particles are suspended at  
29 different wt% and the frozen fraction of each suspension is derived as a function of temperature as represented by the color  
30 bar. To examine the freezing efficiency and compare the different mineral dust types, the results are normalized to the  
31 surface area within each droplet. Experiments were performed at  $1 \text{ K min}^{-1}$  for 40 and 100  $\mu\text{m}$  droplets diameters.  
32 Suspension preparation and evaluation of the surface area are described in the appendix B.

33 The results demonstrate the effect of dust surface area immersed in the droplets on the freezing parameters. The freezing  
34 temperatures increase with increasing surface area and are also reflected in the warming of the median frozen fraction ( $T_{50}$ )  
35 colored in yellow. The spectra of the number of nucleation sites per unit surface area ( $n_s$ ) also support surface area  
36 dependence because all spectra converge to a single line. The  $n_s$  results show the increase of nucleation sites at colder  
37 temperatures. Results from WISDOM are in good agreement with similar analyses from other instruments. In particular,  $n_s$  is  
38 in best agreement with the Leeds-NIPI (Broadley et al., 2012; Murray et al., 2011) results both for K-Feldspar and for Illite-  
39 NX particles. Results of Illite-NX particles are also in good agreement with the Binary instrument (Budke and Koop, 2015)  
40 and reside within the uncertainty of both instruments. The linear trend of few wt% support the assumption that particles in  
41 suspension are uniformly distributed and the droplets contain approximately the same surface area.

#### 42 **3.5.2 Ambient mineral dust**

43 WISDOM can also be used for analyzing collected ambient particles. Mineral dust particles were collected in Rehovot, Israel  
44 (31.9N, 34.8E about 80m AMSL), during dust storm event on 12-13 March 2017). The dust was transported from the Sahara  
45 Desert and North Africa. Size-segregated ambient dust particles were collected on cyclopore polycarbonate filters using a  
46 Micro-orifice Uniform deposit Impactor (MOUDI; MSP Corporation model 110-R, (Marple et al., 1991)), that operated at  
47  $30 \text{ L min}^{-1}$  and for 24 hrs, similarly to Huffman et al. (2013) and Mason et al. (2015). MOUDI has eleven stages with cut  
48 points ( $D_{50}$ ) of 0.056, 0.10, 0.18, 0.32, 0.56, 1.0, 1.8, 3.2, 5.6, 10, and 18  $\mu\text{m}$ . The size distribution of the particles was



49 obtained by Optical Particle Counter (OPC; GRIMM Technologies model 1.109) in the range of 0.25-32  $\mu\text{m}$ , and used for  
50 estimations of surface area immersed in the droplets (further details in Appendix C).  
51 For heterogeneous freezing experiments, a quarter of each filter is placed with 300  $\mu\text{L}$  DDW in 1.5 ml Eppendorf vial and  
52 particles were extracted by intensive dry sonication (Hielcher; model UP200St VialTweeter). In Figure 8, the spectra of the  
53 nucleation sites per unit surface area ( $n_s$ ) of three super-micron stages ( $D_{50}$  of 1.0, 1.8, 3.2  $\mu\text{m}$ ) are presented and  
54 summarized in T1. It is also seen that there are slightly more active sites for the larger particles (3.2  $\mu\text{m}$ ), as their surface  
55 area is higher and there is a higher probability to contain an active site. In Figure 9,  $n_s$  curves of the collected dust is  
56 compared to references of K-feldspar standard particles, analyzed in different instruments (the Leeds-NIPI (Atkinson et al.,  
57 2013), LACIS (Niedermeier et al., 2015)) and to measurements of ambient dust samples, from different locations around the  
58 world, including Israeli settled dust, that was analyzed in the AIDA chamber. Moreover, the freezing of the size resolved  
59 mineral dust analyzed in this study by WISDOM (slope in the temperature range) is consistent with the (grey) polygon that  
60 represents the estimated freezing efficiency for natural concentrations of K-feldspar in internally mixed mineral types  
61 (Atkinson et al., 2013). The results are also in agreement with Niemand et al. (2012), especially between 243 and 249 K. At  
62 warmer temperatures,  $n_s$  of ambient dust in this study showed lower efficiency than in Niemand et al. (2012). This difference  
63 can extend to one order of magnitude in  $n_s$ , and is more pronounced at smaller particles that were analyzed (around 1-1.8 $\mu\text{m}$   
64 diameter). For the larger particles, more nucleating sites are observed. Both the current study and Niemand et al. (2012),  
65 suggest that K-feldspar is involved with the warmer part of their data (>248 K) as the results are consistent with the Atkinson  
66 et al. (2013) scale for ambient samples. The slope of the  $n_s$  derived in this study is similar to the slope from Atkinson et al.  
67 (2013) at warmer temperatures. For the colder regime, the slope is similar to the slope presented by standard K-feldspar  
68 particles in Niedermeier et al., (2015).

### 70 **3.6 WISDOM in comparison to other cold stage instruments**

71 The microfluidics technology used in WISDOM solves some substantial issues inherent in other currently used  
72 instruments: (1) good control of the size and number of monodisperse droplets, (2) fast production of hundreds of nearly  
73 monodisperse droplets minimizes sample sedimentation or agglomeration that may occur in a suspension, leading to a good  
74 estimation of the surface area of the suspended material. Moreover, several droplet diameters can be employed in the same  
75 device without its modification, (3) good statistics achieved by individual analysis of hundreds of droplets, (4) monodisperse  
76 droplets individually analyzed, in contrast to some emulsion techniques (such as Differential Scanning Calorimeter (DSC)),  
77 allow to obtain the frozen fraction at each temperature, and to achieve detailed information about active sites and freezing  
78 rates, (5) the use of oil minimizes possible artefacts from droplets' evaporation, neighbor seeding or vapor transfer due to the  
79 Wegener–Bergeron–Findeisen processes, (6) the small volumes decrease freezing artefacts by impurities, thus allowing to  
80 reach the homogeneous freezing threshold (-37°C), (7) possible investigation of several freezing cycles for the same droplets,

81 (8) the microfluidics method and the small droplet volumes enable working with small sample volumes which can be an  
82 advantage when working with atmospheric samples.

83 WISDOM has a very accurate temperature calibration that spans a wide temperature range, using the eutectic freezing  
84 method. WISDOM most resembles the instrument used by in Edd et al. (2009). However, it seems that issues with  
85 temperature calibration in Edd et al. (2009) led to a temperature offset, and hence different freezing rates. Stan et al. (2009)  
86 achieved better temperature accuracy and high statistics. However, the freezing experiment was conducted in a flow mode,  
87 which is more complicated than in the WISDOM setup and requires complicated modeling. In addition, the cooling rates that  
88 were used were very fast, which induces additional errors. Riechers et al. (2013) had high temperature accuracy as they also  
89 used a DSC. However, they had to collect the droplets from the device as there was no static array option and this may add  
90 further complication and contamination.

91 The microfluidics technology has also disadvantages. These may include: (1) oil may interact with some of the analyzed  
92 particles, possibly leading to biased data, (2) the microchannels are susceptible to clogging, (3) it is not possible to perform  
93 any post analysis to the droplets content after the experiment, (4) the small droplets' volumes reduce the sensitivity to rare  
94 active sites. This may be solved by performing many experiments or by using larger droplets with more surface area within  
95 the droplets.

#### 96 **4 Summary and conclusions**

97 The new setup WISDOM is based on microfluidics technology and its detailed validation is presented. Based on a set of  
98 validation measurements and a good agreement with other instruments, we conclude that WISDOM is a suitable tool for  
99 studying atmospheric ice nucleation, both in homogeneous and heterogeneous immersion freezing modes. Results of  
100 homogeneous freezing correspond to water-activity-based nucleation theory in supercooled droplets and represent well  
101 volume nucleation rates. Heterogeneous freezing in supercooled droplets also agrees well with literature data. Furthermore,  
102 freezing efficiency dependence on the particles surface area within the droplets is clearly observed. Using microfluidics  
103 allows a mass production of picoliter monodisperse droplets using low volumes of suspensions, which can be beneficial for  
104 immersion freezing studies over a wide range of supercooling down to homogenous temperature region. The good  
105 reproducibility of the devices, proved using pure water freezing cycles, enables the recycling of the same device for few  
106 freezing cycles. It is also shown that the temperature uncertainty can be reduced if the temperature calibration includes the  
107 microfluidic devices properties in the working temperature change rates, especially for melting experiments. In this work we  
108 have also demonstrated how WISDOM can be applied for studying the ice nucleation properties of ambient samples that  
109 contain very small quantity of sample. The particles were collected using the MOUDI during Saharan dust storm event.  
110 Results are in correspondence with literature data of ambient dust and further support Atkinson et al. (2013) and the possible  
111 importance of K-feldspar for ice nucleation in clouds, but further analysis of the mineralogy is still needed in order to verify  
112 that.

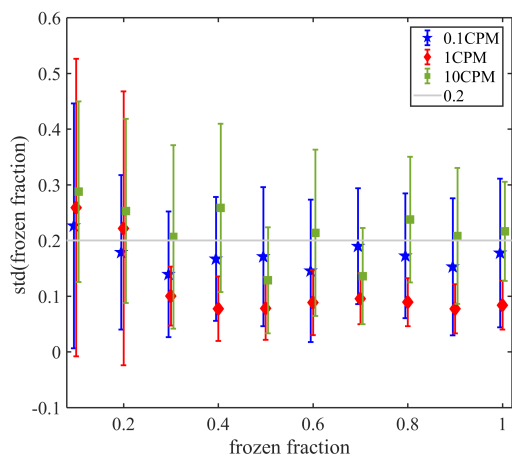
13  
14  
15  
16  
17  
18  
19  
20  
21

The authors declare that they have no conflict of interest.

*Acknowledgements.* We gratefully acknowledge support from the Ice Nuclei Research Unit (INUIT) of the German DFG, to The Helen Kimmel Center for Planetary Sciences, to the De Botton Center for Marine Sciences and for the Weizmann – UK Making Connections Program for funding this work. We also thank Prof. Daniel Knopf, Dr. Carsten Budke, Prof. Thomas Koop, Prof. Ido Braslavski, and Prof. Nir Freidman for their advices and to Prof. Ben Murray and Dr. Heinz Bingemer for sharing K-feldspar and Illite-NX powder standards.

## 22 **Appendix A: Device inter variability over the whole freezing range**

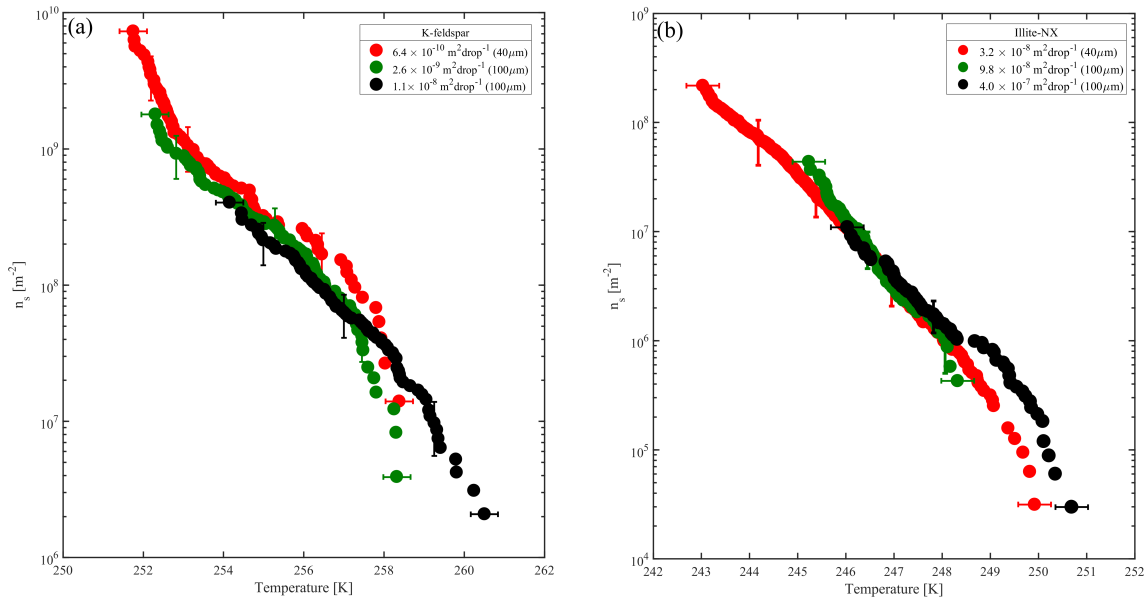
23 Figure A1 presents the reproducibility of the microfluidic devices. For each device, the temperature variation between  
24 different freezing cycles of pure water is presented for the entire range of the freezing at various frozen fractions (0.1 to 1).  
25 These experiments were conducted for three cooling rates,  $0.1 \text{ K min}^{-1}$ ,  $1 \text{ K min}^{-1}$  and  $10 \text{ K min}^{-1}$ . For  $1 \text{ K min}^{-1}$  the device's  
26 variability was the smallest, and the deviation in the results between different cycles was  $< 0.2 \text{ K}$  for most cases. While in  
27 some cycles the temperature was reproducible in  $< 0.05 \text{ K}$ , in other cycles the temperature varied in  $< 0.2 \text{ K}$ . This is not valid  
28 for frozen fractions  $< 0.2$ , where the variability was the highest, as was the case for the other two cooling rates. This may be  
29 due to contaminants that exist in the water or in the devices themselves. The preparation of the devices is mostly inside a  
30 hood, but ambient particles may be trapped during the process. For cooling rate of  $0.1 \text{ K min}^{-1}$ , the variability between the  
31 different cycles was also  $< 0.2 \text{ K}$ , but the variability was higher in comparison to the variability seen at  $1 \text{ K min}^{-1}$ . This can be  
32 explained stochastically and also may be attributed to better resolution of temperature reading during slower cooling rates.  
33 For  $10 \text{ K min}^{-1}$  the variability was between  $0.2 \text{ K}$  and  $0.3 \text{ K}$ . The faster cooling rate may slow the equilibration of droplets'  
34 temperature with respect to the stage (as demonstrated in this work), and also low resolution of temperature reading due to  
35 the fast cooling rate. The variability presented here is also probably affected by the uncertainty of the temperature sensor of  
36 the Linkam stage ( $< 0.25 \text{ K}$ ).



37  
 38 **Figure A1.** Variability of the WISDOM devices for three cooling rates. The markers present the average temperature  
 39 variability for all the devices and the error bars represent one standard deviation. A line is placed at  $\Delta=0.2$  K, the upper value  
 40 which explains the variability in the results of different freezing cycles at 0.1 and 1 K min<sup>-1</sup>.

41 **Appendix B: Suspension preparation and characterization**

42 Illite-NX, ATD and K-feldspar powders were suspended in double distilled water and sonicated twice for 30 seconds with a  
 43 20 second pause, using Hielcher up200St VialTweeter, adjusted especially for Eppendorf vials. K-feldspar suspensions were  
 44 additionally stirred overnight as sonication alone was not enough to achieve a good suspension and intensive sedimentation  
 45 was observed. For validation experiments, suspensions of 0.1 to 1 wt% were used. Figure B1 presents nucleation site  
 46 densities for Illite-NX and K-feldspar particles, and the freezing efficiencies as function of the surface area in the droplets.  
 47 Characterization of the powders can be found in Hiranuma et al. (2015), Marcolli et al. (2007) and in Atkinson et al. (2013)  
 48 and quantification the powders specific surface area was based on N<sub>2</sub> adsorption analysis of Brunauer–Emmett–Teller (BET)  
 49 (Brunauer et al., 1938) using Quantachrome Instruments Nova 2200e and resulted in 1.9±0.6 m<sup>2</sup> g<sup>-1</sup> for the K-feldspar  
 50 powder, 108.6±2.8 m<sup>2</sup> g<sup>-1</sup> for the Illite-NX powder and 37.1±1.4 m<sup>2</sup> g<sup>-1</sup> for the ATD powder. In order to ensure a proper  
 51 analysis of the surface area, and avoid possible surface contaminants as water, surface cleaning was done by degassing the  
 52 powders at 60°C for 3 hours ahead of the BET analysis. Evaluation of the surface area in each droplet was then calculated by  
 53 the wt% which was used, knowing the approximate surface area per mass and assuming that the mass is distributed  
 54 uniformly inside the droplet with the same volume



55

56

57

**Figure B1.** Accumulated active site density spectra ( $n_s$ ) of K-feldspar (a) and Illite-NX (b) particles with different surface areas suspended in water at cooling rate of  $1^\circ\text{C}$  per minute. The error bars are located at three representative frozen fractions, 0.1, 0.5 and 0.9.

58

### Appendix C: Collection of ambient particles during dust storm events in Rehovot

59

60

61

62

63

64

65

66

67

68

69

70

71

72

73

74

The GRIMM measurement was synchronized to the MOUDI stages for the estimation of the total surface area that was collected on the filter for droplets surface area estimation. For that, two base assumptions were made: (1) all the particles that were collected are extracted to the water later used for the freezing experiments, (2) sphericity of the particles. The GRIMM bins are synchronized to the MOUDI stages based on collection efficiency of the MOUDI, obtained from Marple et al. (1991). For example, on certain MOUDI stage, all the particles that own diameter that is larger than the  $D_{50}$  have high chance to be impacted on that stage. All the rest of the sizes, that are smaller in their diameter, will continue to the next stage and will have high chance to deposit there. Hence, the GRIMM's bins were synchronized to the MOUDI  $D_{50}$  stages. For the  $n_s$  calculations, the surface area was based on the number of particles that were measured in a certain bin and their total surface area. To calculate the surface area of a particle (assuming sphericity) in a certain bin, the midpoint of that bin was used as a radius. To calculate the total mass of the particles in each filter, dust density of Quartz was used ( $2.65 \text{ g cm}^{-3}$ ), as this is usually the dominant mineral (Mahowald et al., 2014). The error of the  $n_s$  data is propagated from the error in the frozen fraction, the error of the droplet's volume and the error of the MOUDI's collection efficiency in the different stages, the later was the dominant one.

For control, analysis of blank filter was done. The blanks were sonicated before analysing them and freezing was mostly colder than the freezing temperatures that are presented here and hence no special reduction of the final active sites was done.

76 **References**

- 77 Alpert, P. A., Aller, J. Y., and Knopf, D. A.: Ice nucleation from aqueous NaCl droplets with and without marine diatoms,  
78 *Atmos. Chem. Phys.*, 11, 5539-5555, 2011.
- 79 Ansmann, A., Tesche, M., Althausen, D., Müller, D., Seifert, P., Freudenthaler, V., Heese, B., Wiegner, M., Pisani, G.,  
80 Knippertz, P., and Dubovik, O.: Influence of Saharan dust on cloud glaciation in southern Morocco during the Saharan  
81 Mineral Dust Experiment, *Journal of Geophysical Research: Atmospheres*, 113, n/a-n/a, 2008.
- 82 Atkinson, J. D., Murray, B. J., Woodhouse, M. T., Whale, T. F., Baustian, K. J., Carslaw, K. S., Dobbie, S., O'Sullivan, D.,  
83 and Malkin, T. L.: The importance of feldspar for ice nucleation by mineral dust in mixed-phase clouds, *Nature*, 498, 355-  
84 358, 2013.
- 85 Borgognoni, C. F., Tattini Junior, V., Ayrosa, A. M. I. B., Polakiewicz, B., Leirner, A. A., Maizato, M. J. S., Higa, O. Z.,  
86 Beppu, M. M., and Pitombo, R. N. d. M.: The influence of freezing rates on bovine pericardium tissue Freeze-drying,  
87 *Brazilian Archives of Biology and Technology*, 52, 1493-1504, 2009.
- 88 Broadley, S. L., Murray, B. J., Herbert, R. J., Atkinson, J. D., Dobbie, S., Malkin, T. L., Condliffe, E., and Neve, L.:  
89 Immersion mode heterogeneous ice nucleation by an illite rich powder representative of atmospheric mineral dust, *Atmos.*  
90 *Chem. Phys.*, 12, 287-307, 2012.
- 91 Brunauer, S., Emmett, P. H., and Teller, E.: Adsorption of gases in multimolecular layers, *Journal of the American chemical*  
92 *society*, 60, 309-319, 1938.
- 93 Budke, C. and Koop, T.: BINARY: an optical freezing array for assessing temperature and time dependence of  
94 heterogeneous ice nucleation, *Atmos. Meas. Tech.*, 8, 689-703, 2015.
- 95 Cantrell, W. and Heymsfield, A.: Production of Ice in Tropospheric Clouds: A Review, *Bulletin of the American*  
96 *Meteorological Society*, 86, 795-807, 2005.
- 97 Clegg, S. L., Brimblecombe, P., and Wexler, A. S.: Thermodynamic Model of the System  $H^+-NH_4^+-SO_4^{2-}-NO_3^- -H_2O$  at  
98 Tropospheric Temperatures, *The Journal of Physical Chemistry A*, 102, 2137-2154, Model webpage:  
99 <http://www.aim.env.uea.ac.uk/aim/model2133/model2133a.php>, 1998.
- 00 de Boer, G., Morrison, H., Shupe, M. D., and Hildner, R.: Evidence of liquid dependent ice nucleation in high-latitude  
01 stratiform clouds from surface remote sensors, *Geophysical Research Letters*, 38, n/a-n/a, 2011.
- 02 DeMott, P. J., Prenni, A. J., Liu, X., Kreidenweis, S. M., Petters, M. D., Twohy, C. H., Richardson, M. S., Eidhammer, T.,  
03 and Rogers, D. C.: Predicting global atmospheric ice nuclei distributions and their impacts on climate, *Proceedings of the*  
04 *National Academy of Sciences*, 107, 11217-11222, 2010.
- 05 Edd, J. F., Humphry, K. J., Irimia, D., Weitz, D. A., and Toner, M.: Nucleation and solidification in static arrays of  
06 monodisperse drops, *Lab on a Chip*, 9, 1859-1865, 2009.
- 07 Eddings, M. A. J., M. A.; Gale, B. K.: Determining the optimal PDMS-PDMS bonding technique for microfluidic devices,  
08 *Journal of Micromechanics and Microengineering*, 18, 067001, 2008.
- 09 Farnam, Y., Villani, C., Washington, T., Spence, M., Jain, J., and Jason Weiss, W.: Performance of carbonated calcium  
10 silicate based cement pastes and mortars exposed to NaCl and MgCl<sub>2</sub> deicing salt, *Construction and Building Materials*, 111,  
11 63-71, 2016.
- 12 Field, P. R., Heymsfield, A. J., Shipway, B. J., DeMott, P. J., Pratt, K. A., Rogers, D. C., Stith, J., and Prather, K. A.: Ice in  
13 Clouds Experiment-Layer Clouds. Part II: Testing Characteristics of Heterogeneous Ice Formation in Lee Wave Clouds,  
14 *Journal of the Atmospheric Sciences*, 69, 1066-1079, 2012.
- 15 Hartmann, S., Niedermeier, D., Voigtländer, J., Clauss, T., Shaw, R. A., Wex, H., Kiselev, A., and Stratmann, F.:  
16 Homogeneous and heterogeneous ice nucleation at LACIS: operating principle and theoretical studies, *Atmos. Chem. Phys.*,  
17 11, 1753-1767, 2011.
- 18 Hiranuma, N., Augustin-Bauditz, S., Bingemer, H., Budke, C., Curtius, J., Danielczok, A., Diehl, K., Dreischmeier, K.,  
19 Ebert, M., Frank, F., Hoffmann, N., Kandler, K., Kiselev, A., Koop, T., Leisner, T., Möhler, O., Nillius, B., Peckhaus, A.,  
20 Rose, D., Weinbruch, S., Wex, H., Boose, Y., DeMott, P. J., Hader, J. D., Hill, T. C. J., Kanji, Z. A., Kulkarni, G., Levin, E.  
21 J. T., McCluskey, C. S., Murakami, M., Murray, B. J., Niedermeier, D., Petters, M. D., O'Sullivan, D., Saito, A., Schill, G.

22 P., Tajiri, T., Tolbert, M. A., Welti, A., Whale, T. F., Wright, T. P., and Yamashita, K.: A comprehensive laboratory study  
 23 on the immersion freezing behavior of illite NX particles: a comparison of 17 ice nucleation measurement techniques,  
 24 *Atmos. Chem. Phys.*, 15, 2489-2518, 2015.

25 Hoffer, T. E.: A laboratory investigation of droplet freezing, *Journal of Meteorology*, 18, 766-778, 1961.

26 Hoose, C. and Möhler, O.: Heterogeneous ice nucleation on atmospheric aerosols: a review of results from laboratory  
 27 experiments, *Atmos. Chem. Phys.*, 12, 9817-9854, 2012.

28 Huffman, J. A., Prenni, A. J., DeMott, P. J., Pöhlker, C., Mason, R. H., Robinson, N. H., Fröhlich-Nowoisky, J., Tobo, Y.,  
 29 Després, V. R., Garcia, E., Gochis, D. J., Harris, E., Müller-Germann, I., Ruzene, C., Schmer, B., Sinha, B., Day, D. A.,  
 30 Andreae, M. O., Jimenez, J. L., Gallagher, M., Kreidenweis, S. M., Bertram, A. K., and Pöschl, U.: High concentrations of  
 31 biological aerosol particles and ice nuclei during and after rain, *Atmos. Chem. Phys.*, 13, 6151-6164, 2013.

32 IPCC: Climate Change 2013: The Physical Science Basis. Contribution of Working Group I to the Fifth Assessment Report  
 33 of the Intergovernmental Panel on Climate Change, Cambridge University Press, Cambridge, United Kingdom and New  
 34 York, NY, USA, 2013.

35 Knopf, D. A. and Lopez, M. D.: Homogeneous ice freezing temperatures and ice nucleation rates of aqueous ammonium  
 36 sulfate and aqueous levoglucosan particles for relevant atmospheric conditions, *Physical Chemistry Chemical Physics*, 11,  
 37 8056-8068, 2009.

38 Koop, T., Luo, B., Tsias, A., and Peter, T.: Water activity as the determinant for homogeneous ice nucleation in aqueous  
 39 solutions, *Nature*, 406, 611-614, 2000.

40 Koop, T. and Zobrist, B.: Parameterizations for ice nucleation in biological and atmospheric systems, *Physical Chemistry  
 41 Chemical Physics*, 11, 10839-10850, 2009.

42 Kuan-Ting, O. and Wood, R.: Exploring an approximation for the homogeneous freezing temperature of water droplets,  
 43 *Atmos. Chem. Phys.*, 16, 7239-7249, 2016.

44 Mahowald, N., Albani, S., Kok, J. F., Engelstaeder, S., Scanza, R., Ward, D. S., and Flanner, M. G.: The size distribution of  
 45 desert dust aerosols and its impact on the Earth system, *Aeolian Research*, 15, 53-71, 2014.

46 Marcolli, C., Gedamke, S., Peter, T., and Zobrist, B.: Efficiency of immersion mode ice nucleation on surrogates of mineral  
 47 dust, *Atmos. Chem. Phys.*, 7, 5081-5091, 2007.

48 Marple, V. A., Rubow, K. L., and Behm, S. M.: A Microorifice Uniform Deposit Impactor (MOUDI): Description,  
 49 Calibration, and Use, *Aerosol Science and Technology*, 14, 434-446, 1991.

50 Mason, R. H., Chou, C., McCluskey, C. S., Levin, E. J. T., Schiller, C. L., Hill, T. C. J., Huffman, J. A., DeMott, P. J., and  
 51 Bertram, A. K.: The micro-orifice uniform deposit impactor–droplet freezing technique (MOUDI-DFT) for measuring  
 52 concentrations of ice nucleating particles as a function of size: improvements and initial validation, *Atmos. Meas. Tech.*, 8,  
 53 2449-2462, 2015.

54 Murray, B. J., Broadley, S. L., Wilson, T. W., Atkinson, J. D., and Wills, R. H.: Heterogeneous freezing of water droplets  
 55 containing kaolinite particles, *Atmos. Chem. Phys.*, 11, 4191-4207, 2011.

56 Murray, B. J., Broadley, S. L., Wilson, T. W., Bull, S. J., Wills, R. H., Christenson, H. K., and Murray, E. J.: Kinetics of the  
 57 homogeneous freezing of water, *Physical Chemistry Chemical Physics*, 12, 10380-10387, 2010.

58 Murray, B. J., O'Sullivan, D., Atkinson, J. D., and Webb, M. E.: Ice nucleation by particles immersed in supercooled cloud  
 59 droplets, *Chemical Society Reviews*, 41, 6519-6554, 2012.

60 Nagare, B., Marcolli, C., Welti, A., Stetzer, O., and Lohmann, U.: Comparing contact and immersion freezing from  
 61 continuous flow diffusion chambers, *Atmos. Chem. Phys.*, 16, 8899-8914, 2016.

62 Neethirajan, S., Kobayashi, I., Nakajima, M., Wu, D., Nandagopal, S., and Lin, F.: Microfluidics for food, agriculture and  
 63 biosystems industries, *Lab on a Chip*, 11, 1574-1586, 2011.

64 Niedermeier, D., Augustin-Bauditz, S., Hartmann, S., Wex, H., Ignatius, K., and Stratmann, F.: Can we define an asymptotic  
 65 value for the ice active surface site density for heterogeneous ice nucleation?, *Journal of Geophysical Research:  
 66 Atmospheres*, 120, 5036-5046, 2015.

67 Niedermeier, D., Hartmann, S., Shaw, R. A., Covert, D., Mentel, T. F., Schneider, J., Poulain, L., Reitz, P., Spindler, C.,  
 68 Clauss, T., Kiselev, A., Hallbauer, E., Wex, H., Mildnerberger, K., and Stratmann, F.: Heterogeneous freezing of droplets  
 69 with immersed mineral dust particles – measurements and parameterization, *Atmos. Chem. Phys.*, 10, 3601-3614, 2010.

70 Niemand, M., Möhler, O., Vogel, B., Vogel, H., Hoose, C., Connolly, P., Klein, H., Bingemer, H., DeMott, P., Skrotzki, J.,  
71 and Leisner, T.: A Particle-Surface-Area-Based Parameterization of Immersion Freezing on Desert Dust Particles, *Journal of*  
72 *the Atmospheric Sciences*, 69, 3077-3092, 2012.

73 Possner, A., Ekman, A. M. L., and Lohmann, U.: Cloud response and feedback processes in stratiform mixed-phase clouds  
74 perturbed by ship exhaust, *Geophysical Research Letters*, 44, 1964-1972, 2017.

75 Pruppacher, H. R., Klett, J. D., and Wang, P. K.: *Microphysics of Clouds and Precipitation*, *Aerosol Science and*  
76 *Technology*, 28, 381-382, 1998.

77 Riechers, B., Wittbracht, F., Hutten, A., and Koop, T.: The homogeneous ice nucleation rate of water droplets produced in a  
78 microfluidic device and the role of temperature uncertainty, *Physical Chemistry Chemical Physics*, 15, 5873-5887, 2013.

79 Rosenfeld, D. and Woodley, W. L.: Deep convective clouds with sustained supercooled liquid water down to -  
80 37.5[thinsp][deg]C, *Nature*, 405, 440-442, 2000.

81 Sackmann, E. K., Fulton, A. L., and Beebe, D. J.: The present and future role of microfluidics in biomedical research,  
82 *Nature*, 507, 181-189, 2014.

83 Schmitz, C. H. J., Rowat, A. C., Koster, S., and Weitz, D. A.: Dropspots: a picoliter array in a microfluidic device, *Lab on a*  
84 *Chip*, 9, 44-49, 2009.

85 Schnaiter, M., Järvinen, E., Vochezer, P., Abdelmonem, A., Wagner, R., Jourdan, O., Mioche, G., Shcherbakov, V. N.,  
86 Schmitt, C. G., and Tricoli, U.: Cloud chamber experiments on the origin of ice crystal complexity in cirrus clouds,  
87 *Atmospheric Chemistry and Physics*, 16, 5091-5110, 2016.

88 Stan, C. A., Schneider, G. F., Shevkoplyas, S. S., Hashimoto, M., Ibanescu, M., Wiley, B. J., and Whitesides, G. M.: A  
89 microfluidic apparatus for the study of ice nucleation in supercooled water drops, *Lab on a Chip*, 9, 2293-2305, 2009.

90 Stöckel, P., Weidinger, I. M., Baumgärtel, H., and Leisner, T.: Rates of Homogeneous Ice Nucleation in Levitated H<sub>2</sub>O and  
91 D<sub>2</sub>O Droplets, *The Journal of Physical Chemistry A*, 109, 2540-2546, 2005.

92 Ullrich, R., Hoose, C., Möhler, O., Niemand, M., Wagner, R., Höhler, K., Hiranuma, N., Saathoff, H., and Leisner, T.: A  
93 New Ice Nucleation Active Site Parameterization for Desert Dust and Soot, *Journal of the Atmospheric Sciences*, 74, 699-  
94 717, 2017.

95 Vali, G.: Quantitative Evaluation of Experimental Results on the Heterogeneous Freezing Nucleation of Supercooled  
96 Liquids, *Journal of the Atmospheric Sciences*, 28, 402-409, 1971.

97 Vali, G., DeMott, P. J., Möhler, O., and Whale, T. F.: Technical Note: A proposal for ice nucleation terminology, *Atmos.*  
98 *Chem. Phys.*, 15, 10263-10270, 2015.

99 Whale, T. F., Murray, B. J., O'Sullivan, D., Wilson, T. W., Umo, N. S., Baustian, K. J., Atkinson, J. D., Workneh, D. A., and  
00 Morris, G. J.: A technique for quantifying heterogeneous ice nucleation in microlitre supercooled water droplets, *Atmos.*  
01 *Meas. Tech.*, 8, 2437-2447, 2015.

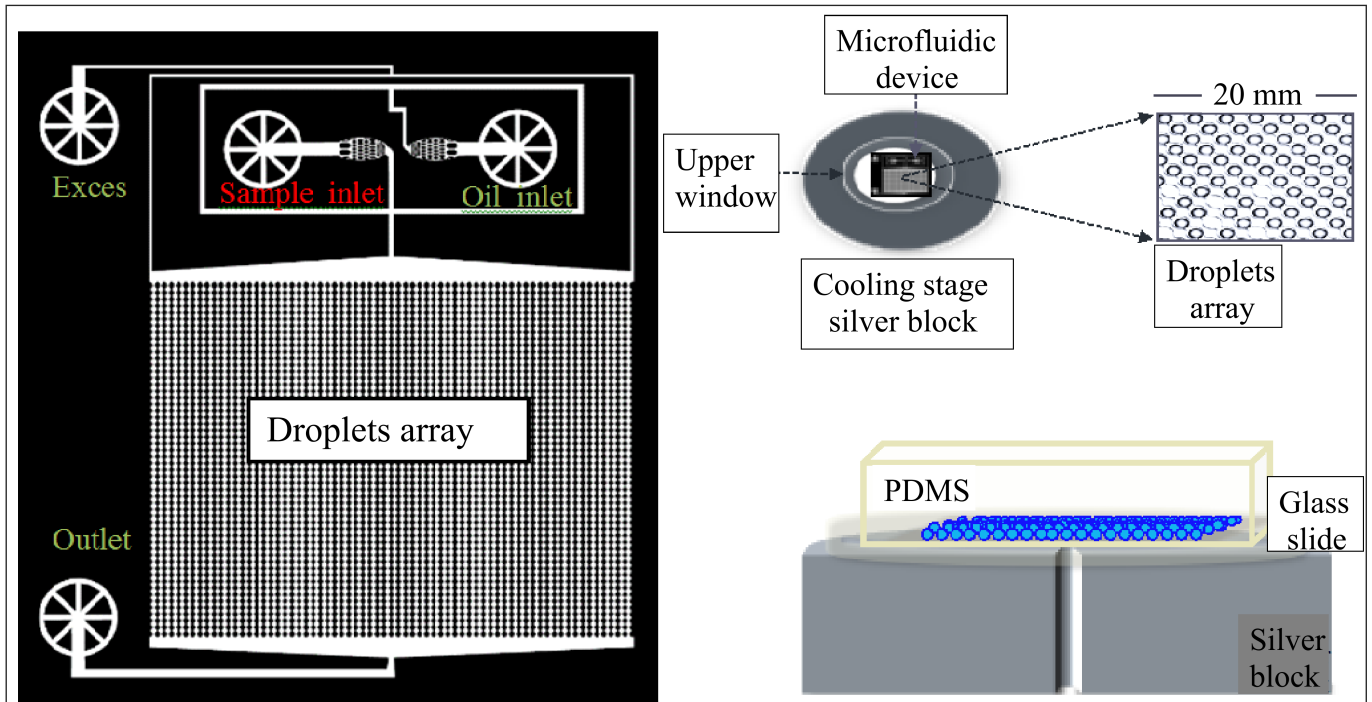
02 Whitesides, G. M.: The origins and the future of microfluidics, *Nature*, 442, 368-373, 2006.

03 Zobrist, B., Marcolli, C., Peter, T., and Koop, T.: Heterogeneous Ice Nucleation in Aqueous Solutions: the Role of Water  
04 Activity, *The Journal of Physical Chemistry A*, 112, 3965-3975, 2008.

05

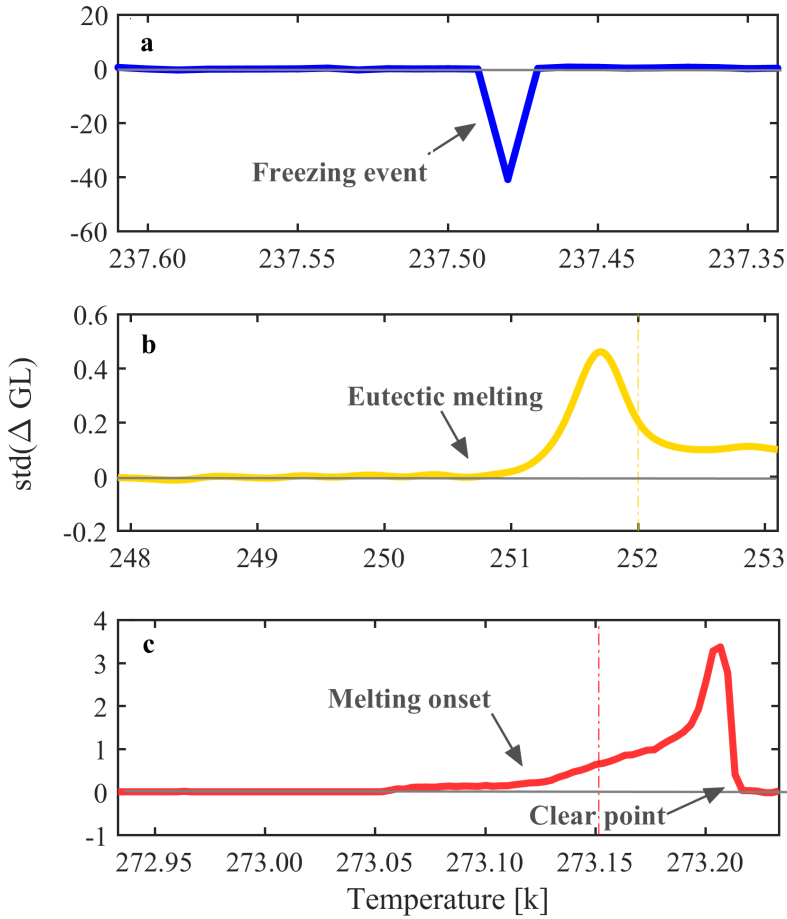
06





07  
 08  
 09  
 10  
 11  
 12  
 13  
 14  
 15

**Figure 1:** The WISDOM setup. a) The design of the microfluidic device is based on Schmitz et al. (2009). Aqueous solutions (including the sample) and oil are connected through the inlets and merge in a junction to generate monodisperse droplets. Subsequently, droplets flow into a trap array and settle in them as the flow is stopped. The device is transferred into a cooling stage for subsequent freezing experiments. b) upper and c) side views of the device, which is made of PDMS, plasma glued to a microscope glass slide, placed over the cooling silver block.



16

17

18

19

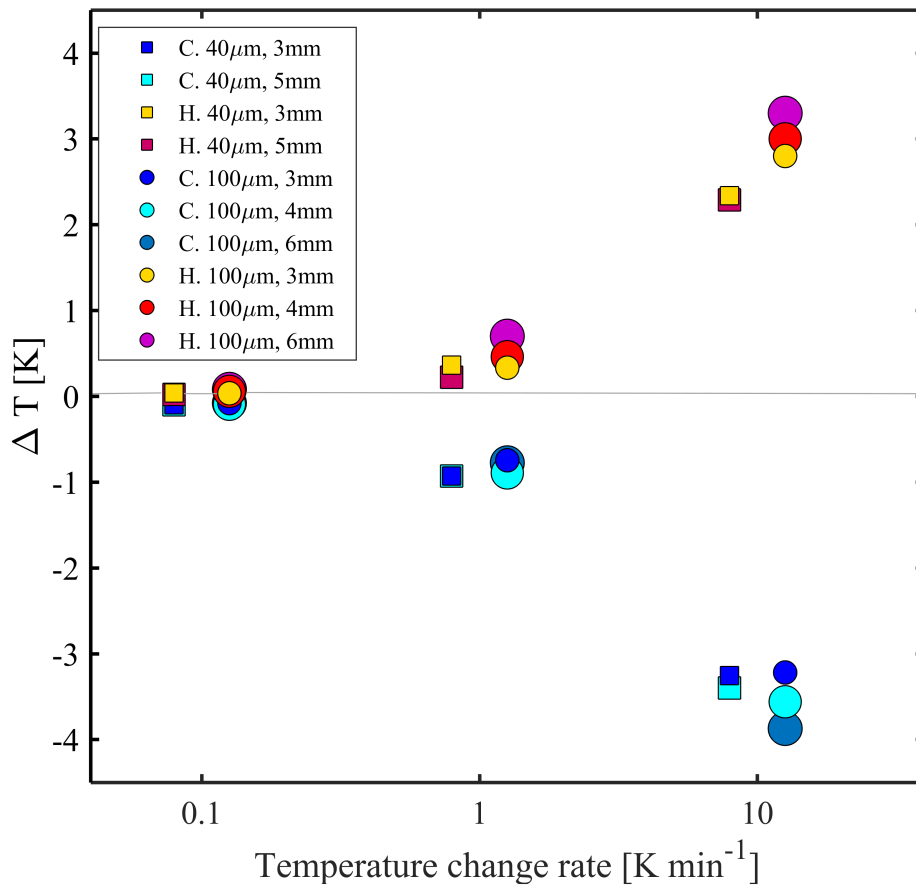
20

21

22

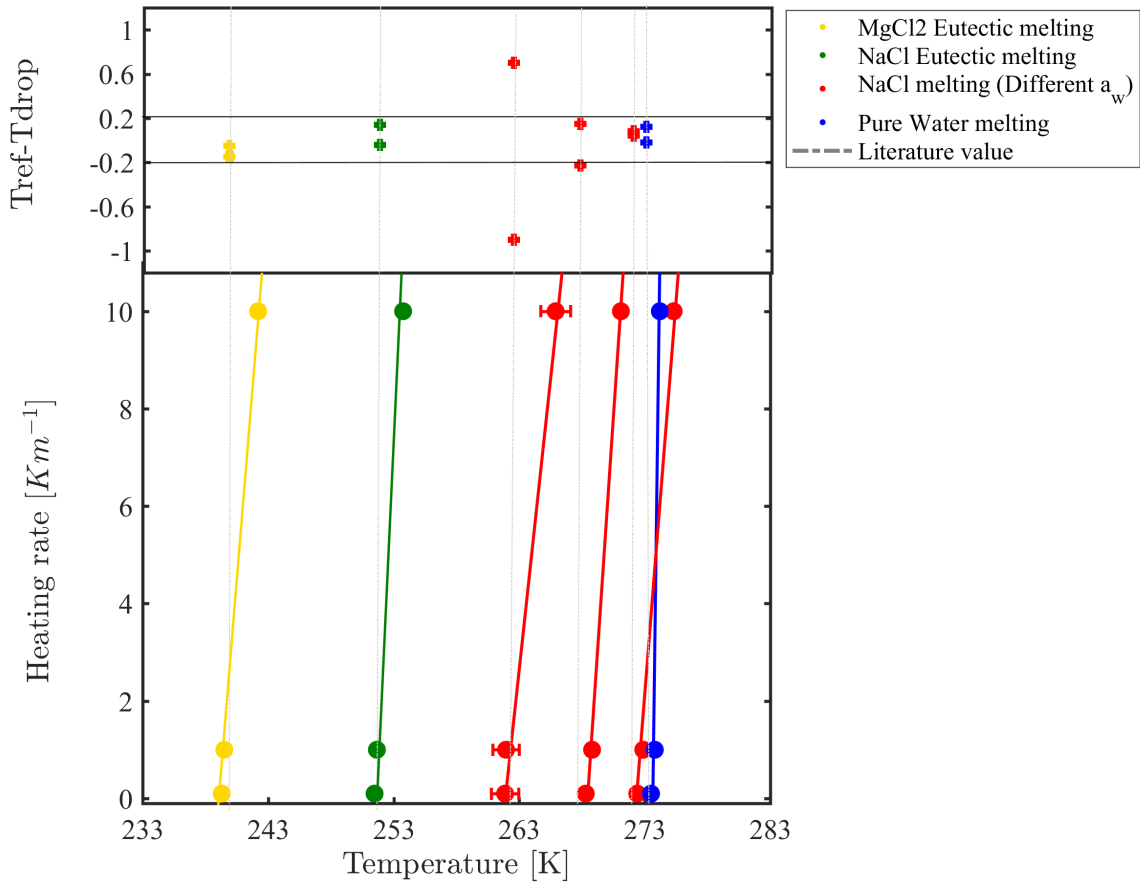
23

**Figure 2:** Spectra of different phase transition events as observed in WISDOM. a) freezing, b) eutectic melting, and c) melting onset and clear point (liquefaction) are the mean of all sampled droplets in a single experiment. The phase transition is defined optically by the brightness information obtained by the gray level of the image pixels.  $\text{std}(\Delta \text{GL})$  describes the standard error of the difference in mean GL for two consecutive frames. At the beginning of the experiment the noise level is studied and freezing, or melting are detected only if  $\text{std}(\Delta \text{GL})$  is as least 5 times greater than the noise std level. Freezing and melting examples are for pure water droplets and the eutectic melting example is for aqueous solution droplets of NaCl. Eutectic melting point of NaCl and pure water melting point are marked by the yellow and red lines in b and c, correspondingly. In all cases the droplets diameter was 100  $\mu\text{m}$ .



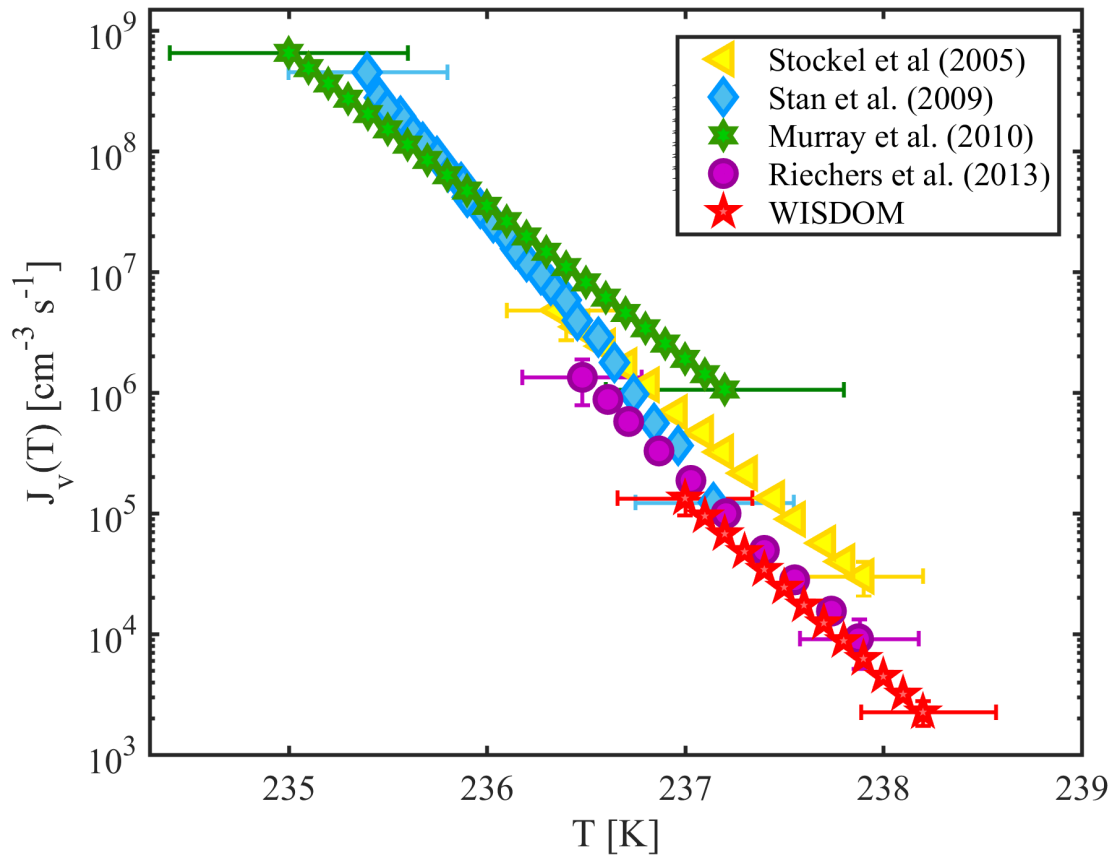
24  
25

26 **Figure 3.** The temperature difference ( $\Delta T$ ), defined as the temperature difference between the stage temperature and the droplet  
 27 extrapolated temperature at equilibrium conditions at different cooling (heating) rates. Freezing and melting points of pure water are  
 28 represented by circles and squares (40 and 100  $\mu\text{m}$  droplet diameter, in correspondence) for different PDMS thicknesses and are  
 29 represented by different colors. C denotes cooling and H denotes heating. Droplets are close to equilibrium with the stage temperature at  
 30 rates  $< 0.1 \text{ K min}^{-1}$  and  $\Delta T$  increases with increasing temperature change rate and with the PDMS height.



31

32 **Figure 4.** Temperature calibration by melting points of eutectic solutions and pure water droplets for different heating rates. Calibration is  
 33 presented for 100  $\mu\text{m}$  droplets with 4 mm PDMS thickness. The onsets of pure water droplets are also considered. Eutectic melting is used  
 34 for the colder temperature range ( $<253$  K) while clear point (liquefaction) at various water activities is taken for the warmer temperature  
 35 range. The upper panel presents the temperature difference between the reference value and the cooling stage temperature after calibration.  
 36 Most of the differences are within the range  $\pm 0.2$  K.



37

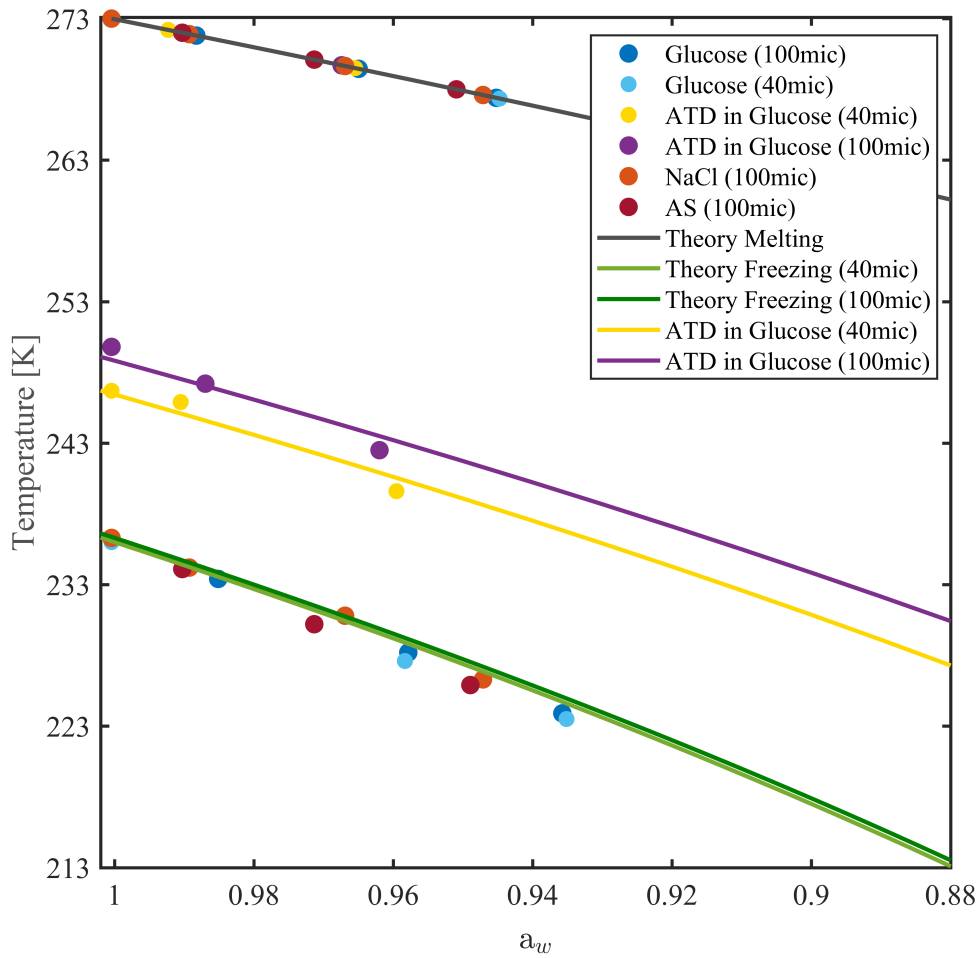
38

39

40

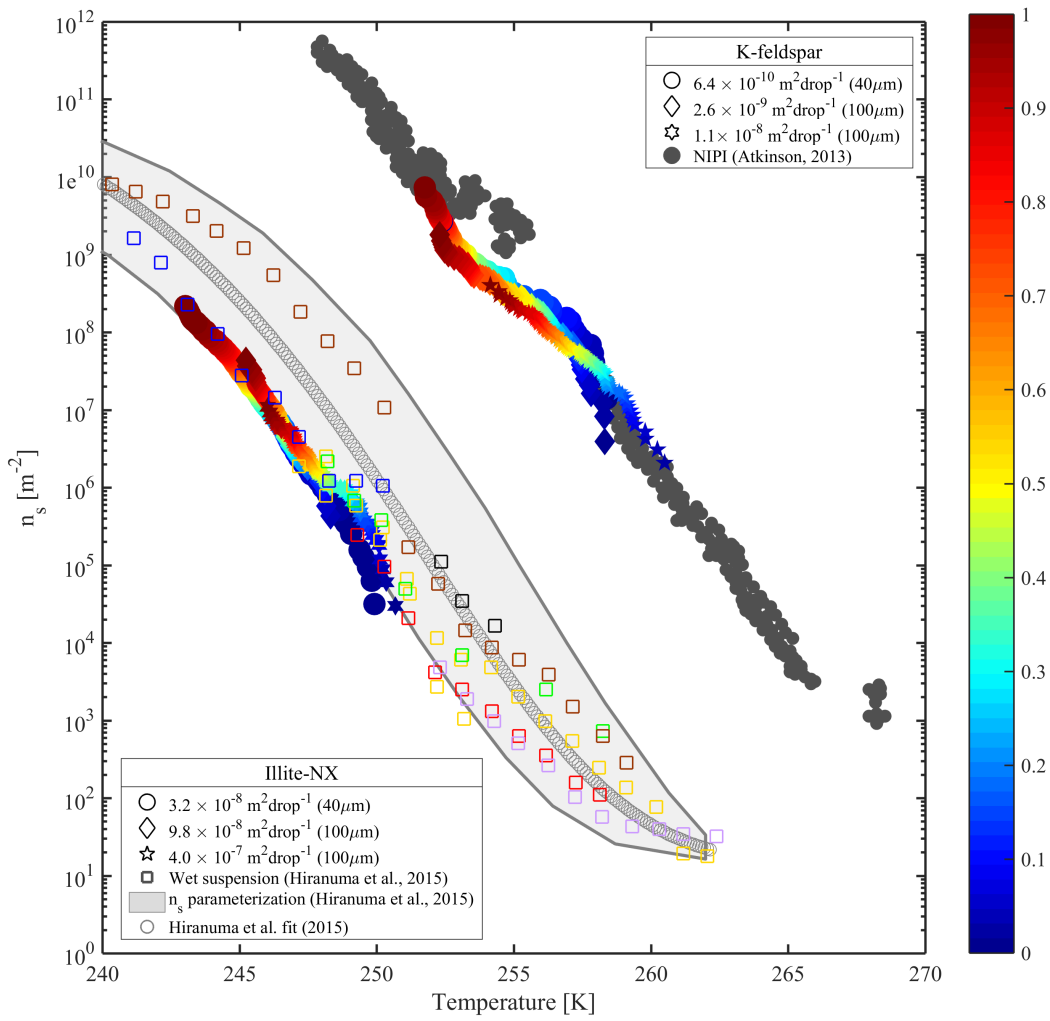
41

**Figure 5.** The volume-dependent homogeneous freezing of pure water, derived for 100  $\mu\text{m}$  droplets with 4 mm PDMS height. WISDOM rates are compared to relevant literature data. The obtained fit from WISDOM is  $J_{v(T)} = \exp(-3.4T + 817.6)$ . Temperature uncertainty for WISDOM is  $\pm 0.3$  K.



42

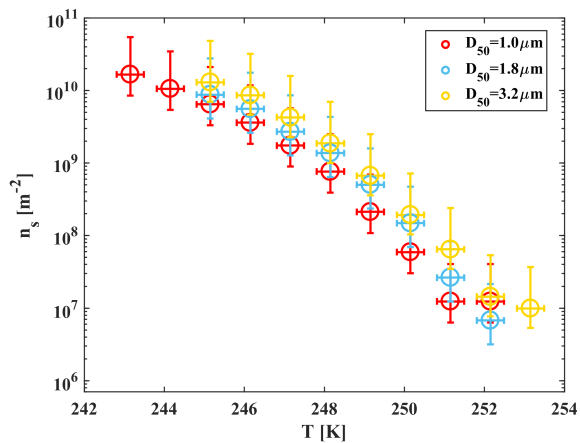
43 **Figure 6.** Homogeneous and heterogeneous ice nucleation temperatures for 40 and 100  $\mu\text{m}$  aqueous solution droplets as a function of  
 44 solution water activity. Freezing and melting curves are derived from Koop et al. (2000). Heterogeneous ice nucleation is performed with  
 45 0.1 wt % ATD particles immersed in the droplets.  
 46



47  
48

49 **Figure 7.** Accumulated active site density spectra ( $n_s$ ) of K-feldspar and Illite-NX particles as a function of temperature from validation  
50 experiments of immersion freezing in WISDOM. Frozen fraction values are represented by a color bar, for few surface area values that are  
51 exposed in 40 and 100  $\mu\text{m}$  droplets. The dependence of the nucleation site density on the surface area is illustrated here. WISDOM  
52 uncertainties, propagated from surface area estimation and measured frozen fraction errors, are included within the size of the markers. For  
53 validation, previous immersion freezing measurements are also presented (Hiranuma et al. (2015) and Atkinson et al. (2013)). T-binned  
54 data ( $1^\circ\text{C}$ ) normalized by the BET surface area from Hiranuma et al. (2015) is presented in the color squares, only for wet suspension  
55 analysis (Binary (red), CSU-IS (orange), Leeds-NIPI (purple), M-AL (green), M-WT (black), NC-State-CS (brown) and CU-RMCS  
56 (blue)). Hiranuma et al. log fit and  $n_s$  (BET) parameterization are also presented.

57  
58  
59



61

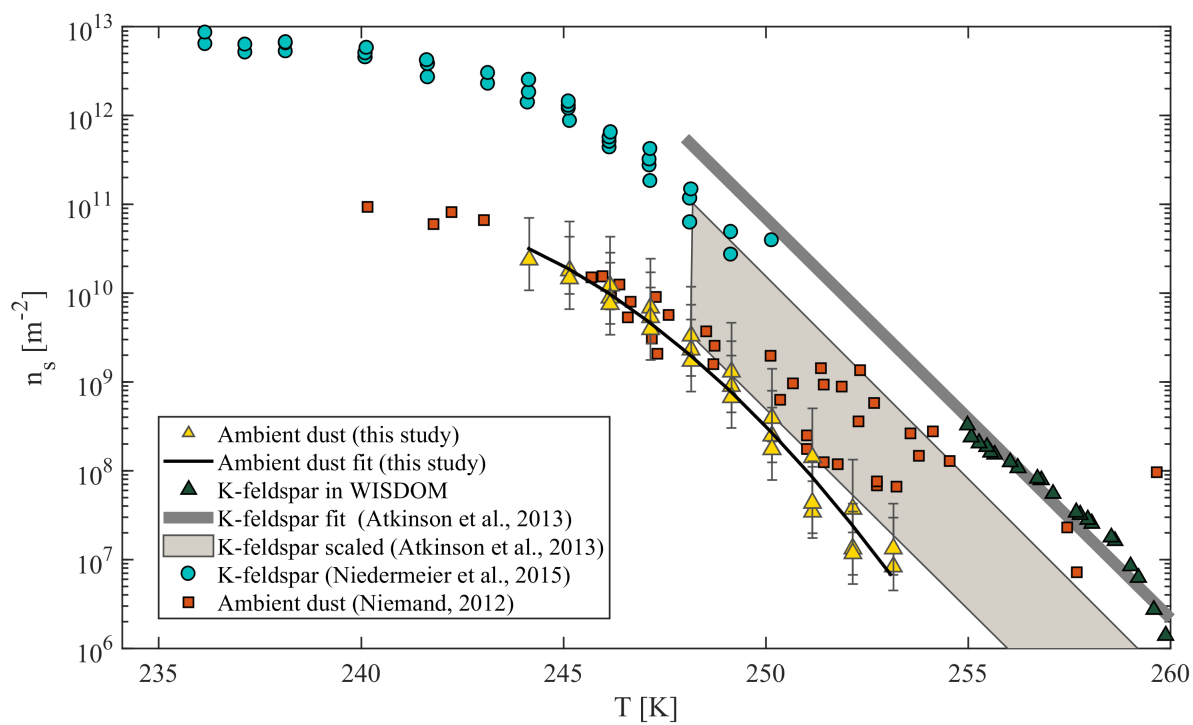
62 **Figure 8.** Accumulated active site density spectra ( $n_s$ ) of ambient super-micron mineral dust particles collected in Israel during Saharan  
 63 dust events in 2017, for three different sampling stages of the MOUDI;  $D_{50}$  of 1, 1.8 and  $3.2 \mu\text{m}$ .

64

65

66

67



68



69 **Figure 9.** Accumulated active site density spectra ( $n_s$ ) of ambient super-micron mineral dust particles collected in Israel during dust event  
70 in 2017 for three MOUDI stages that were analyzed with  $D_{50}$  of 1, 1.8 and 3.2  $\mu\text{m}$ . The fit  $\ln(n_s) = -0.057T^2 + 24.68T - 2.93$   
71 ( $R^2=0.98$ ) is also presented. References of K-feldspar standard particles activated in WISDOM, Leeds-NIPI (Atkinson et al., 2013) and  
72 LACIS (Niedermeier et al., 2015) instruments are presented, as well as ambient dust particles that were analyzed in AIDA and included  
73 Israeli dust (Niemand et al., 2012).

74 **Table 1. Summary of immersion freezing experiments performed for WISDOM validation.**

		Droplets diameter [ $\mu\text{m}$ ]	SA [ $\text{m}^2 \text{drop}^{-1}$ ]	$T_{50}$ [K]	BET [ $\text{m}^2 \text{g}^{-1}$ ]
<b>Illite-NX</b>					
	0.2wt%	95.1 $\pm$ 3.6	$3.2 \times 10^{-10}$	246.4	
	0.8wt%	96.1 $\pm$ 2.9	$9.8 \times 10^{-08}$	247.8	108.6 $\pm$ 2.8
	1wt%	38.2 $\pm$ 2.4	$4.0 \times 10^{-07}$	245.4	
<b>K-feldspar</b>					
	0.2wt%	99.6 $\pm$ 2.8	$6.4 \times 10^{-10}$	255.3	
	0.8wt%	98.2 $\pm$ 2.6	$2.6 \times 10^{-09}$	257.0	1.9 $\pm$ 0.6
	1wt%	39.8 $\pm$ 2.4	$1.1 \times 10^{-08}$	253.3	
<b>0.1 wt% ATD in glucose</b>					
	$a_w=1$	98.1 $\pm$ 3.8	$1.8 \times 10^{-08}$	250.0	
	$a_w=0.987$	101.2 $\pm$ 2.9	$2.0 \times 10^{-08}$	247.5	
	$a_w=0.962$	99.1 $\pm$ 4.6	$1.9 \times 10^{-08}$	242.9	37.1 $\pm$ 1.4
	$a_w=1$	38.3 $\pm$ 3.2	$1.1 \times 10^{-09}$	246.2	
	$a_w=0.991$	39.9 $\pm$ 3.3	$1.2 \times 10^{-09}$	240.2	
	$a_w=0.959$	37.3 $\pm$ 2.8	$1.0 \times 10^{-09}$	236.3	
<b>DS</b>					
<b>12-13/03/17</b>					
$D_{50}$	1.0	89.9 $\pm$ 4.3	$3.6 \times 10^{-10}$	247.5	-
[ $\mu\text{m}$ ]	1.8	95.6 $\pm$ 9.6	$6.0 \times 10^{-10}$	248.8	
	3.2	89.4 $\pm$ 10.8	$2.6 \times 10^{-10}$	248.7	

75  
76  
77  
78  
79  
80  
81